Sensors and Actuators B 247 (2017) 780–790

Contents lists available at ScienceDirect

Sensors and Actuators B: Chemical

journal homepage: www.elsevier.com/locate/snb

The influence of the electrode dimension on the detection sensitivity of electric cell–substrate impedance sensing (ECIS) and its mathematical modeling

Xudong Zhang[a,*], William Wang[b], Anis Nurashikin Nordin[c], Fang Li[d], Sunghoon Jang[e], Ioana Voiculescu[a]

[a] Mechanical Engineering Department, City College of New York, New York, NY, USA
[b] Amity Regional High School, Woodbridge, CT, USA
[c] Electrical and Computer Engineering Department, International Islamic University, Malaysia
[d] Mechanical Engineering Department, New York Institute of Technology, New York, NY, USA
[e] Computer Engineering Technology Department, New York City College of Technology, New York, NY, USA

ARTICLE INFO

Article history:
Received 4 November 2016
Received in revised form 27 January 2017
Accepted 11 March 2017
Available online 16 March 2017

Keywords:
ECIS
Sensitivity
Model
Electrodes
Design

ABSTRACT

Detection sensitivity is a crucial criterion in the design and application of ECIS sensors. The influence of sensing electrode dimension on detection sensitivity is investigated in this paper. Eight types of ECIS sensors were fabricated, and their experimental results reveal that smaller-radius working electrodes generate more sensitive impedance shift to cell density change. Also, the smaller radius of working electrodes yield higher impedance values, which improves signal-to-noise ratio. In a range from 1.0 mm to 3.5 mm, the distance between the working and counter electrodes does not affect impedance measurements. However, the distance should be large enough to prevent the current from directly bypassing the cells between the electrodes. A mathematical model has been developed to analyze the distribution of electric potential and current over the sensing electrodes of ECIS sensors, which is helpful in understanding the mechanisms of ECIS. This mathematical model, supported by experimental data and finite element analysis, is able to illustrate a quantitative relationship between cell impedance and cell characteristics. This model can be used to optimize the design of ECIS sensors and interpret cell behavior.

1. Introduction

The electric cell–substrate impedance sensing (ECIS) technique can analyze cell migration, attachment, invasion, proliferation, and barrier function [1–5]. The measured impedance data can provide information on cell membrane capacitance, cytoplasm conductivity, and intercellular junction condition, which are all related to cell behavior and morphology [1–9]. Live cells attach and spread on the surface of ECIS electrodes after seeding, and behave like an insulating medium that limits the current flow between the electrodes, thus the measured impedance increase between the electrodes [10–18]. The measured impedance will stabilize after the cells form a monolayer on the sensor. Changes in measured impedance correspond to variations of the monolayer caused by cell–cell interactions, cell–substrate interactions, or changing cell electrical properties due to chemical, biological, or physical stimuli [19].

Detection sensitivity is a crucial criterion in the applications of ECIS sensors. It depends on sensor configuration, such as electrode dimension and the distance between the electrodes. Wang et al. have fabricated coplanar interdigital ECIS sensors using different working electrode dimensions to investigate their detection sensitivity [20]. However, no study has been reported about the influence of sensor dimension on the detection sensitivity of circular coplanar ECIS sensors.

Mathematical modeling can provide more information that cannot be obtained directly through experimental data, including cell membrane capacitance, dielectric resistance, and morphology, which are useful to analyze the cell behavior. The membrane capacitance of nerve cells plays an important functional role in synaptic integration and signal propagation [21]. The embryonic carcinoma cells show specific dielectric resistance profiles during

* Corresponding author.
E-mail addresses: xzhang19@citymail.cuny.edu (X. Zhang), wangwi@stanford.edu (W. Wang), anisnn@iium.edu.my (A.N. Nordin), fli08@nyit.edu (F. Li), sJang@citytech.cuny.edu (S. Jang), voicules@ccny.cuny.edu (I. Voiculescu).

http://dx.doi.org/10.1016/j.snb.2017.03.047
0925-4005/

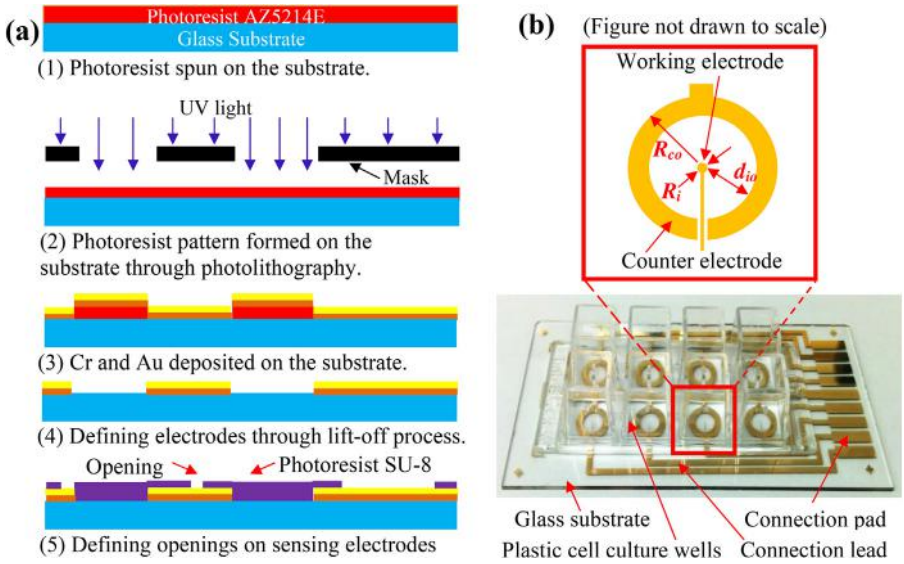

Fig. 1. (a) Illustration of ECIS sensor fabrication. (b) The array of eight ECIS sensors.

induced differentiation [22]. Several mathematical models have been developed to analyze the relationship between measured cell impedance and cell characteristics [1–10,23–28]. Some of these models assumed that cell membrane was a capacitor, cell cytoplasm a resistor, and cell impedance calculated as a combination of the capacitors and resistors [24–28]. Furthermore, the current flows either through the cells or around the cells. However, in reality, the current may switch from one path to another, creating a hybrid path. Other models have considered all of these three paths [1–10,23]. Nevertheless, these models assumed that the current flows radially between the ventral surface of the cell and the substratum and the electric potential is constant inside the cell. However, if the current flow through the entirety of the cell, the electric potential cannot be constant inside the cell. Therefore, Ohm's law invalidates this assumption.

In this paper, ECIS sensor arrays were fabricated to investigate the influence of sensor dimension on detection sensitivity. Also, a new mathematical model has been developed to illustrate the distribution of current and electrical potential, and the relationship between measured cell impedance and cell characteristics.

2. Materials and methods

2.1. Cell culture and preparation

Bovine aortic endothelial cells (BAECs, VEC Technologies, Rensselaer, NY) were used in this study. The BAECs were cultured in Minimum Essential Medium (MEM, GIBCO, Grand Island, NY) with 10% fetal bovine serum (FBS, GIBCO, Grand Island NY) under standard mammalian cell culturing conditions (37 °C and 5% CO_2).

2.2. Fabrication of ECIS sensor arrays

The ECIS arrays were fabricated on glass by thin film deposition and lift-off photolithography technique, as shown in Fig. 1(a). After patterning the photoresist AZ5214E (MicroChemicals, Somerville, NJ), 10 nm chromium (Cr) followed by 100 nm gold (Au), was thermally evaporated onto the substrate to form the sensor's electrodes. After the lift-off process, the photoresist SU-8 (Microchem, Westborough, MA) was used to partially cover the connection leads of sensor array. The sensor arrays were treated with 95% sulfuric acid at 80 °C for 10 s followed by washing with DI water, and was treated with 10% APTES at 50 °C for 2 h to increase the surface biofunctionality [29]. Finally, commercial cell culture wells (Lab-Tek 8-well culture wares) were glued onto sensor arrays. Fig. 1(b) shows the fabricated ECIS sensor array and its configuration. Table 1 shows the configuration of ECIS sensors. R_i is the radius of the working electrode, R_{co} the outer radius of the counter electrode, d_{io} the distance between the edges of the electrodes, S_1 and S_2 are the area of the working and counter electrode respectively.

Table 1
Configuration of ECIS sensors.

Type	R_i (μm)	R_{co} (μm)	d_{io} (μm)	S_1 (mm^2)	S_2 (mm^2)
1	100	4500	3500	0.0314	22.9022
2	150	4500	3500	0.0707	21.7634
3	200	4500	3500	0.1257	20.6089
4	250	4500	3500	0.1964	19.4386
5	300	4500	3500	0.2827	18.2527
6	400	4500	3500	0.5027	15.8336
7	100	2915	1000	0.0314	22.8935
8	100	3420	2000	0.0314	22.8909

2.3. Experimental system setup

Impedance analyzer Agilent 4294 and ECIS Z system (Applied Biophysics, Troy, NY) were used to measure the cell impedance. The Tektronix oscilloscope DPO2014B was used to monitor the AC signal applied on cells. Two MAXIM DG408 Multiplexers, controlled by an NI USB-6008 multifunction data acquisition card, were used as a 16-channel multiplexer between the impedance analyzer and the sensor arrays. The NI USB-6008 and Agilent 4294 were controlled by LabView programs to acquire impedance from ECIS sensor arrays. The experimental setup is shown in Fig. 2. The ECIS sensor arrays, seeded with mammalian cells, were kept inside an incubator with 37 °C and 5% CO_2 during the impedance measurement.

2.4. Finite elements analysis of the ECIS

There are mainly five physical layers in an ECIS sensor. From the bottom to the top of the sensor, they are the sensing substrate layer, electrode–electrolyte layer, thin cell culture medium layer, cell layer, and cell culture medium layer. A simplified axisymmetric finite element ECIS model for a few cells was established to analyze the distribution of electric potential and current on thin cell culture medium layer, as shown in Fig. 3. A gap was assumed

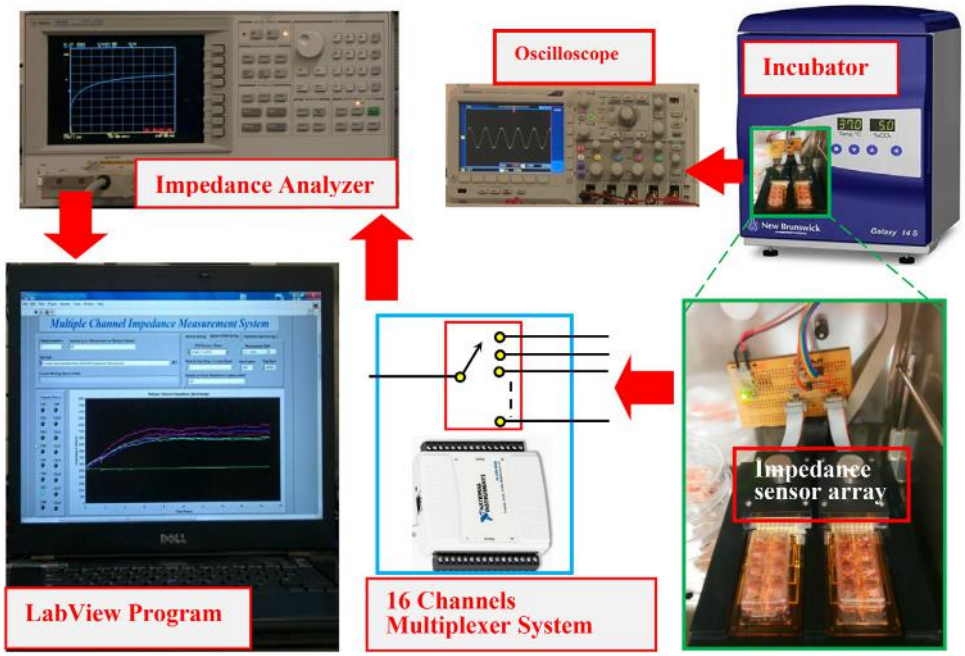

Fig. 2. Experimental setup of cell impedance measurement.

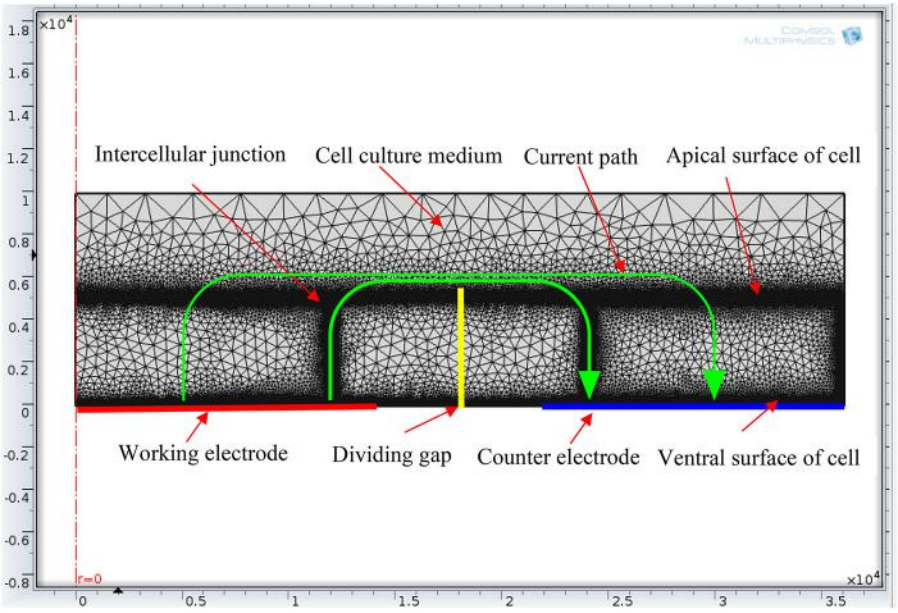

Fig. 3. Mesh of the finite element model of ECIS sensor with cells.

Table 2
Parameters used in calculating the impedance of cells.

Parameters	Relative permittivity	Conductivity (S/m)	Values
Cell membrane	20	5×10^{-8}	Thickness: 5×10^{-9} m
Cell cytoplasm	80	0.4	
Cell culture medium	80	1.6	
Cell radius (r_c)			12×10^{-6} m
Cell thickness (h_2)			5×10^{-6} m
Average distance between ventral surface of cell and electrode–electrolyte interface (h_1)			100×10^{-9} m
Radius of working electrode (R_i)			100×10^{-6} m
Average horizontal distance of intercellular junction (d)			20×10^{-9} m
Intercellular junction coefficient (α)			0.5
Charge transfer resistance of electrode–electrolyte interface (R_{ct})			$5.03 \times 10^6\ \Omega\,cm^2$
Double layer capacitance of electrode–electrolyte interface (C_{dl})			$60\ \mu F/cm^2$

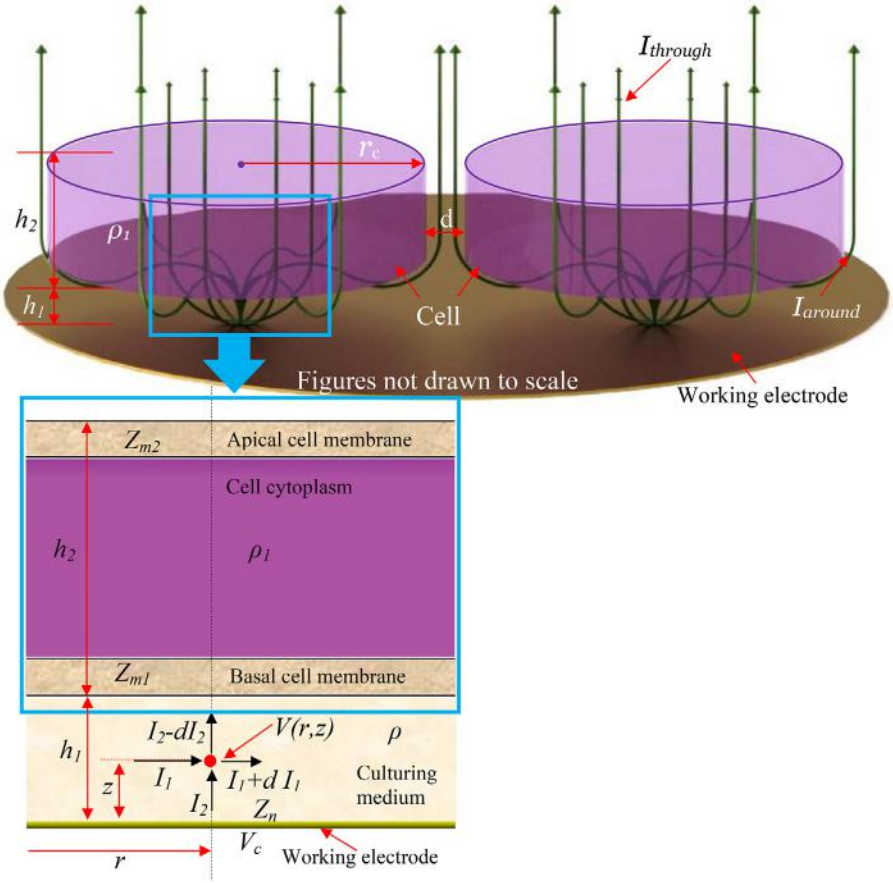

Fig. 4. Illustration of cell impedance sensing on a working electrode. The electric potential on the red point at the coordinate (r, z) is $V(r, z)$. ρ and ρ_1 are the resistivity of the cell culture medium and cytoplasm respectively. Z_{m1}, Z_{m2} and Z_n are the specific impedance of the basal cell membrane, apical cell membrane, and electrode–electrolyte interface respectively (in $\Omega\,m^2$). h_1 is the average distance between the ventral surface of cell and electrode–electrolyte interface. h_2 is the average thickness of the cell. d is the average horizontal distance between adhesive cells. V_c is the electrical potential on the working electrode.

to divide the working electrode zone and counter electrode zone, shown as the yellow line in Fig. 3. That gap prevents the current from transmitting from the working electrode to counter electrode directly without passing through the cells. The parameters related to the electrical properties and geometric dimension used in the finite element model and the following mathematical model were the same, as shown in Table 2.

3. Mathematical model of electric cell–substrate impedance sensing (ECIS)

A new model was proposed to analyze the distribution of current and electric potential. The graphical representations of the current paths were established in cylindrical coordinates (r, θ, z) as shown in Fig. 4. Because the model is axisymmetric, this model was simplified into 2-dimensional coordinates (r, z),

$$\rho\left(\frac{I_1}{2\pi rz}e_r + \frac{I_2}{\pi r^2}e_z\right) = E \tag{1}$$

$$\frac{\partial V}{\partial r}e_r + \frac{\partial V}{\partial z}e_z = -E \tag{2}$$

$$I_1 + I_2 = I_1 + dI_1 + I_2 - dI_2 \tag{3}$$

where: ρ is the resistivity of the cell culture medium. I_1 and I_2 are the current flowing through the point (r, z) in the r and z directions respectively. e_r and e_z are unit vectors in the r and z directions. E is the electric field at any point (r, z). V is the electric potential at the point (r, z). dI_1 and dI_2 are the infinitesimally small current of I_1 and I_2. dI_1 and dI_2 have the same sign.

Eq. (1) can be obtained from the differential form of Ohm's law, $I_1/2\pi rz$ and I_2/π^2 are the current density in the r and z directions respectively. The gradient of electric potential is related to the electric field, and it can be decomposed into $\partial V/\partial r$ and $\partial V/\partial z$, as shown in Eq. (2). According to Kirchhoff's circuit law, the sum of currents flowing into the node (r, z) is equal to the sum of the current flowing out of the node, as shown in Eq. (3).

$$\frac{2\pi z}{-\rho}\left(\frac{\partial V}{\partial r} + r\frac{\partial^2 V}{\partial r^2}\right) - \frac{2\pi r}{-\rho}\left(\frac{\partial V}{\partial z}\right) = 0 \tag{4}$$

$$V(r, z) = AI_0(2cr)\,e^{2c^2z^2} + D \tag{5}$$

where: $I_0(2cr)$ is the modified Bessel function of the first kind, and A, D and c are coefficients.

After substituting Eq. (1) and (2) into Eq. (3), the governing equation of the electric potential at any point (r, z) can be obtained, as shown in Eq. (4). Eq. (5) is the solution of Eq. (4). When the variable z is held constant, Eq. (5) is the same as the solution of electric potential in Dr. Giaever's ECIS model [3,23].

Boundary Condition 1:

$$V_c - V(r = 0, z = h_1) = \lim_{r\to 0}\frac{Z_n}{\pi r^2}I_2 \tag{6}$$

Boundary Condition 2:

$$V(r_e, z = 0) = 0 \tag{7}$$

Boundary Condition 3:

$$I_j = I_1(r_c, h_1) + I_2(r_c, h_1) \tag{8}$$

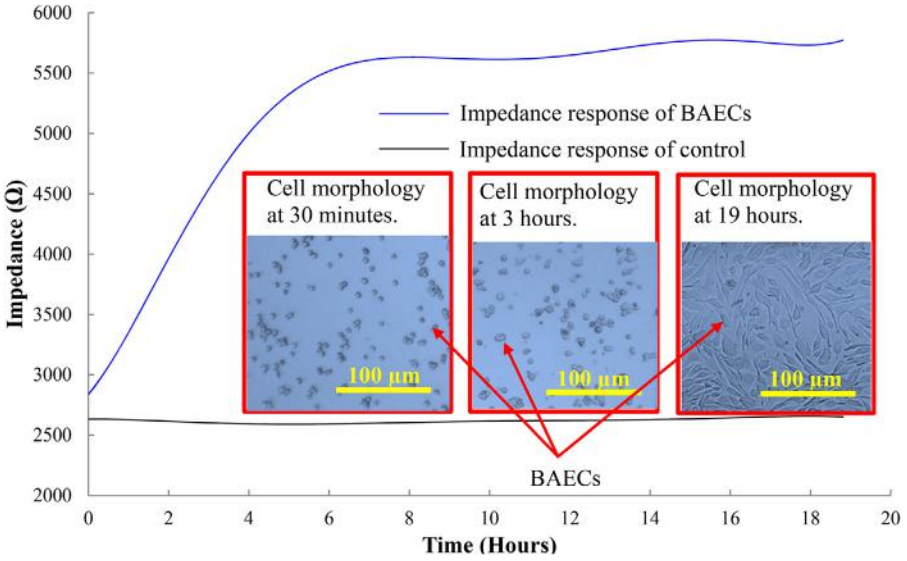

Fig. 5. Impedance response of BAECs measured by an ECIS sensor array at 8000 Hz and the image of cell morphology.

where: V_c is the electric potential applied on the working electrode. Z_n is the specific impedance of the electrode–medium interface (unit $\Omega\,m^2$). r_e is the radius of the positive electrode. h_1 is the average distance between the ventral surface of cell and electrode–electrolyte interface. h_2 is the average thickness of the cell layer. d is the average horizontal distance of the intercellular junction. The vertical intercellular junction length is αh_2 ($0 \le \alpha \le 1$). r_c is the average radius of a single cell. I_j is the current flowing through the intercellular junction gap.

Three boundary conditions were needed to determine the three unknown coefficients, A, D and c in Eq. (5). First, the relationship between electric potential difference and current at the points ($r = 0$, $z = 100$ nm) should be consistent with Ohm's law, as shown in Eq. (6). Secondly, the electric potential at the edge of the positive (working) electrode should be zero, as shown in Eq. (7). Finally, the current flowing through the intercellular junction gap (I_j) is mainly from I_1 and I_2 at the edge of the cell, as shown in Eq. (8). I_j is equal to the quotient of the electric potential difference on the edge of the intercellular junction over the resistance of intercellular junction. These three coefficients A, D and c were calculated using the parameters shown in Table 2 [30–36].

3.1. Quantification of the impedance of electrode–electrolyte interface and cell culture medium

The equivalent circuit of electrode–electrolyte interface is a double layer capacitance (C_{dl}), shunted by a Faradic impedance [37–39]. The double layer capacitance is 60 μF/cm^2 with the solution relative permittivity around 80 [40]. The Faradic impedance comprises a charge transfer resistance (R_{ct}) and a Warburg impedance (Z_w) in series. The value of R_{ct} was determined by the electron transfer rate and was estimated to be $5.03 \times 10^6\ \Omega\,cm^2$ [41]. Z_w was related to the mass diffusion process occurring in the electrode–electrolyte interface and was neglected due to the characteristics of the electrode material [42–44]. The specific impedance of electrode-electrode interface (Z_n) can be calculated, as shown in Eq. (9).

$$Z_n = \frac{R_{ct}}{2\pi f C_{dl} \times R_{ct} + 1} \tag{9}$$

where: f is the measurement frequency.

For a round planar working electrode with an infinitely large counter electrode, the impedance of the culture medium (R_s) can be estimated as $\rho/4R_i$ [42,45–47]. For a finite size of counter electrode, R_s can be calculated by integrating the series resistance of electrolyte shells moving outward from the working to counter electrode, as shown in Eq. (10) [43,48].

$$R_s = \int_{R_i}^{R_i+d_{io}} dR = \int_{R_i}^{R_i+d_{io}} \frac{\rho}{2\pi r h} dr = \frac{\rho}{2\pi h} \ln \frac{R_i + d_{io}}{R_i} \tag{10}$$

where: ρ is the resistivity of the electrolyte. h is the height of cell culture medium in culture wells (5 mm in this study).

The impedance generated from the cell culture medium between the ventral surface of cell and electrode–electrolyte interface ($Z_{cell-sub}$) also needed to be considered. $Z_{cell-sub}$ can be calculated by dividing the electric potential difference between the edge and center of a single cell by the total current flowing through and around the cell as shown in Eq. (11).

$$Z_{cell_sub} = \frac{V(0,h_1) - V(r_c,h_1)}{I_2 + I_j} = \frac{\rho(I_0 - 1)\sqrt{\sigma^2 + (2\pi f\varepsilon\varepsilon_0)^2}}{\pi(4c^2h_1)[r_c^2 I_0\sqrt{\sigma^2} + (2\pi f\varepsilon\varepsilon_0)^2 + \frac{r_c d}{\rho\alpha h_2}\left(\rho_1 h_2\sqrt{\sigma^2} + (2\pi f\varepsilon\varepsilon_0)^2 + 2t\right)(2I_0 + 2cr_c I_1)]} \tag{11}$$

where: $V(0, h_1) - V(0, h_1)$ is the difference in electric potential between the edge and center of a single cell, which was expressed in Eq. (5). I_2 is the current flowing through a single cell and can be calculated from Eq. (1). I_j is the current flowing through the intercellular junction gap, which is also equal to the current flowing around the cell. I_j can be calculated from Eq. (8). ρ_1 is the resistivity of cell cytoplasm. t and σ are the thickness and conductivity of the cell membrane respectively. ε is the relative permittivity of the cell membrane. ε_0 is the vacuum permittivity, which is 8.85×10^{-12} F/m.

3.2. The calculated impedance of a single cell

The impedance of a single cell ($Z_{single\ cell}$) can be calculated by dividing the electric potential difference between the apical and

ventral surfaces of a single cell by the total current flowing through and around the cell, as shown in Eq. (12).

$$Z_{\text{sin gle cell}} = \frac{V(r_c, h_1) - V(r_c, h_1 + h_2)}{I_2 + I_j} = \frac{\left(\rho_1 h_2 \sqrt{\sigma^2 + (2\pi f \varepsilon \varepsilon_0)^2} + 2t\right)(2I_0 + 2cr_c I_1)}{2\pi \left[r_c^2 I_0 \sqrt{\sigma^2 + (2\pi f \varepsilon \varepsilon_0)^2} + \frac{r_c d}{\rho \alpha h_2}\left(\rho_1 h_2 \sqrt{\sigma^2 + (2\pi f \varepsilon \varepsilon_0)^2} + 2t\right)(2I_0 + 2cr_c I_1)\right]} \quad (12)$$

where: $V(r_c, h_1) - V(r_c, h_1 + h_2)$ is the difference of electric potential between the apical cell membrane and the basal cell membrane.

3.3. The calculated impedance of the cell monolayer covering an ECIS sensor

In this model, the impedance of the ECIS sensor (Z) can be calculated as the sum of the impedance generated at the working electrode zone ($Z_{working}$), the impedance generated at the

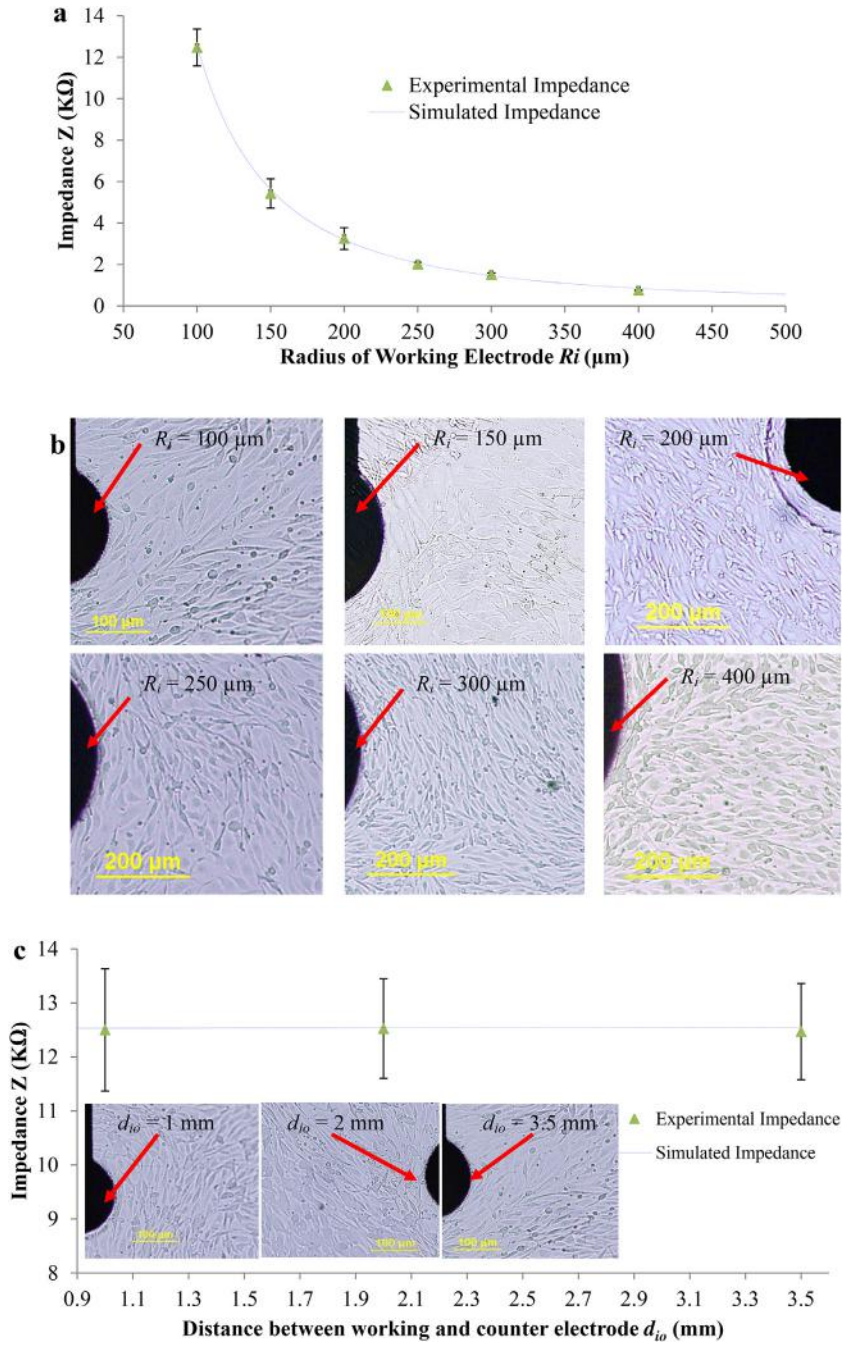

Fig. 6. (a) Relationships between R_i and experimental impedance, and between R_i and simulated impedance at 8000 Hz (n = 4–6, d_{io} = 3.5 mm). (b) BAEC monolayer on ECIS sensors with different R_i (d_{io} = 3.5 mm). (c). Relationships between d_{io} and experimental impedance, and between d_{io} and simulated impedance, measured at 8000 Hz (n = 6–7, R_i = 100 μm). The three images show the cell morphology of BAECs on the ECIS sensors with d_{io} of 1 mm, 2 mm and 3.5 mm respectively. (For interpretation of the references to color in the text, the reader is referred to the web version of this article.)

counter electrode zone ($Z_{counter}$), and R_s, as shown in Eq. (13).

$$Z = Z_{working} + Z_{counter} + R_s = \left(\frac{1}{S_1} + \frac{1}{S_2}\right)\left[Z_n + \frac{S(Z_{single\,cell} + Z_{cell\_sub})}{n}\right] + R_s \quad (13)$$

where: S_1 and S_2 are the surface area of the working and counter electrode respectively. S is the total surface area of the ECIS sensor, which contains the working electrode, counter electrode and non-electrode area. Z is the calculated impedance from the ECIS sensor. n is the number of cells seeded on the ECIS sensor. The rest of parameters were noted in the previous sections.

4. Results and discussion

4.1. The impedance response from the fabricated ECIS sensor arrays

The optimal measurement frequency allows the sensors to obtain the largest difference in measured impedance between a sample with and without cells [19]. In this study, the optimal measurement frequency was 8000 Hz in both the mathematical and finite element models. The inherent impedance of the Au/Cr electrodes was 19 Ω at 8000 Hz measured by microwave probe station and impedance analyzer, as shown in Fig. S1. The inherent impedance of the sensor can be neglected, because it is much lower than the measured cellular impedance in the thousands of ohms. Fig. 5 shows the BAECs impedance responses and morphology in the first 19 h after seeding onto the ECIS sensor array. The cell impedance increased until the 8 h mark, which indicates the initial formation of a loose monolayer, and the impedance plateaued until the end of the experiment. After the formation of the cell monolayer was confirmed under microscope, the impedance readings were used to represent the impedance of the cell monolayer for cell-based assays.

4.2. The design guidelines of electrode dimensions of ECIS sensors

4.2.1. The radius of working electrode (R_i)

The experimental and simulated impedance using different R_i are shown in Fig. 6(a). Fig. 6(b) illustrates the cell morphology on those sensors. The experimental and simulated impedances using smaller R_i sensors are usually higher.

The ECIS sensors usually contain working and counter electrodes. There are many paths for the current to flow through the cell monolayer between the working and counter electrodes. The counter electrodes are used to provide adequate current paths to enable circuit connection, which needs the counter electrode to have adequate sensing area. The smaller R_i working electrode provides less current paths, which increases the corresponding impedance. The higher impedance values can improve data quality by increasing signal-to-noise ratio. It is useful particularly for observing small changes in cell behavior. However, the working electrode should not be too small in order to measure an adequate number of cells and to guarantee sufficient cell-to-cell contact area.

The maximum difference between the simulated and the experimental impedances is calculated to be 13.29% in Fig. 6(a). That difference is acceptable when considering the fluctuation of experimental impedance. The simulated impedance curve matches the experimental data closely for the R_i range from 100 μm to 400 μm, as shown in Fig. 6(a). The consistency of the simulated impedance with the experimental impedance validates this model's ability to optimize the R_i according to the range of measured cell number and expected output impedance level during sensor designing.

4.2.2. The distance between the edges of the sensing electrodes (d_{io})

The distance between the edges of the sensing electrodes (working electrodes and counter electrodes) (d_{io}) is another factor that needs to be considered in designing ECIS sensors. The green triangles show the relationships between d_{io} and the experimental impedance as shown in Fig. 6(c). When the d_{io} changed from 1000 μm to 3500 μm, the average experimental impedance slightly changed from 12.50 kΩ to 12.52 kΩ. This indicates d_{io} in the range of 1000 μm to 3500 μm only has a little influence on the impedance. d_{io} influenced the impedance of medium, which is only a small portion of measured impedance. Thus, the d_{io} cannot dramatically influence the measured impedance. However, d_{io} should not be too small to avoid the current from flowing under the cell monolayer between sensing electrodes.

The blue line in Fig. 6(c) shows the relationship between d_{io} and the simulated impedance calculated using Eq. (13). In Eq. (13), the natural logarithm of the quotient of ($R_i + d_{io}$) and R_i make the influence of d_{io} on simulated impedance more slightly. Consequently, the d_{io} only slightly influence the simulated impedance. The simulated impedance is consistent with the experimental data with 0.63% as the maximum difference. The consistency of the simulated impedance with the experimental impedance validates the model.

4.3. The influence of electrode dimensions on the detection sensitivity of ECIS

Detection sensitivity in cell-based assays is reflected by the fineness of impedance response to cell changes. Because the standard commercial ECIS sensor (Applied Biophysics, Troy, NY) have a 125 μm R_i. Sensors with R_i of 100 μm and 150 μm (Types 1 and 2 in Table 1b) were used to study the influence of working electrode dimension on detection sensitivity. 90,000, 100,000 and 110,000 cells/cm^2 cell confluent densities were used to observe the relationship between cell density and impedance. Fig. 7(a) shows the impedance shifts to the cell density changes using the sensors with R_i of 100 μm and 150 μm. Fig. 7(b) shows the corresponding cell morphology on the ECIS sensors. When the cell density change is 10,000 cells/cm^2 (from 90,000 to 100,000 cells/cm^2), the impedance increased 597 Ω and 350 Ω for the sensors with R_i of 100 μm and 150 μm respectively. When the cell density change is 20,000 cells/cm^2 (from 90,000 to 110,000 cells/cm^2), the impedance increased 1336 Ω and 880 Ω for the sensors with R_i of 100 μm and 150 μm respectively. The sensors with smaller R_i provided larger impedance changes to the same cell density changes. Thus, the sensors with smaller R_i are able to detect finer changes in cell density. Therefore, ECIS sensors with smaller dimension working electrodes illustrate better detection sensitivity on changes in cell density. Another benefit is that smaller R_i requires fewer cells in cell-based assays.

4.4. Analyzing the distribution of current density beneath the ventral surface of cells from the mathematical model and finite element model

In several ECIS models, the current was assumed to flow radially between the ventral surface of the cell and the substratum [1–5]. The distribution of electric potential was calculated from Eq. (5) and the resultant equipotential lines are nearly vertical, as shown in Fig. 8(a). Because the direction of current density is the same as the gradient of the electric potential, the current is proven to flow radially between the ventral surface of cell and the

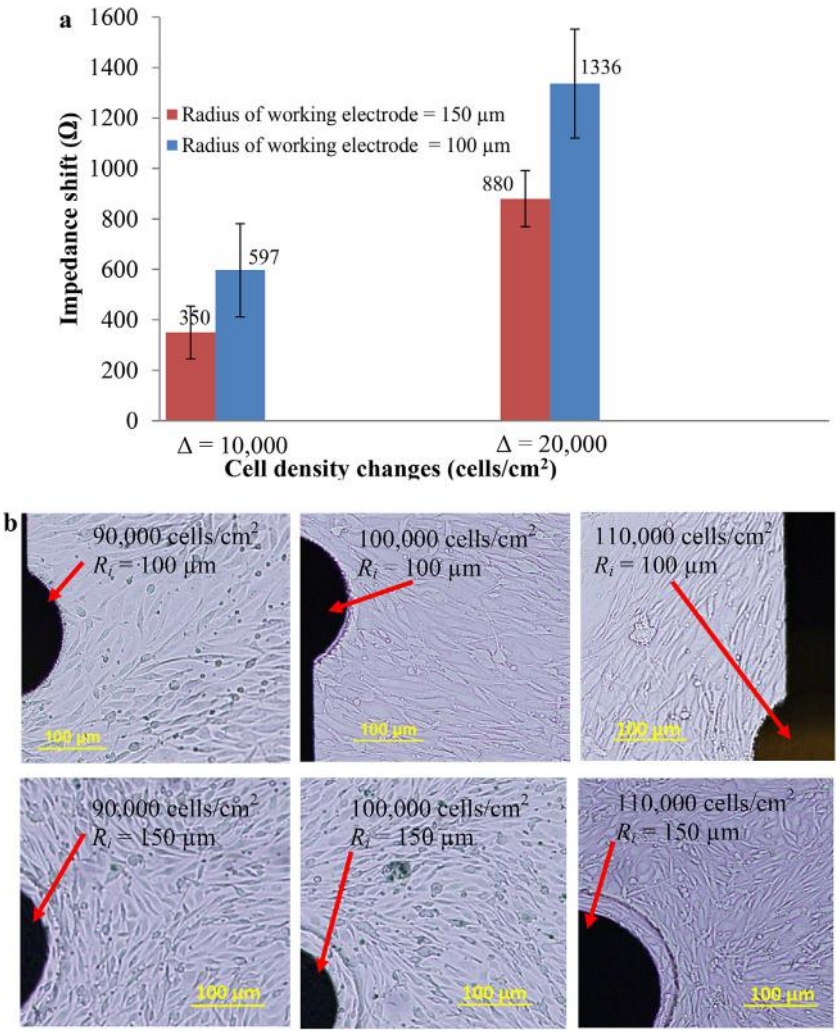

Fig. 7. (a) Impedance shifts to cell density changes with sensors' R_i of 100 μm and 150 μm (n = 3). The cell density change from 90,000 cells/cm^2 to 100,000 or 110,000 cells/cm^2. (b) Cell morphology with 90,000, 100,000, and 110,000 cells/cm^2 cell densities on ECIS sensors (R_i = 100 μm and R_i = 150 μm).

electrode–electrolyte interface. The density of equipotential lines in areas far from the cell's center is higher than that in the center, meaning the amount of current flowing around the cell is larger than that through the cell. The distribution of electric potential and current density was also analyzed by the finite element model, as shown in Fig. 8(b). It shows that the current flows radially, which is consistent with the analyzed results from the mathematical model.

The quantative comparison of electric potential distribution calculated from the mathematical and finite element model is shown in Fig. 8(c). Both distributions were 50 nm over the electrode–electrolyte interface from the center of the cell to its edge. The maximum difference in electric potential between the mathematical and finite element model is 4.3% (at 12 μm on the horizontal axis). Perhaps d_{io} was too short in the finite element model compared to that in mathematical model. As a result, the electric potential decreases with larger extent in the finite element model.

4.5. The relationship between impedance and cell morphology and electrical properties from the mathematical modeling

Cell morphology, including the thickness and radius of cells, and electrical properties, including membrane capacitance and cytoplasm resistivity, can affect impedance. The volume of an endothelial single cell was assumed to be constant during a specific period with the cell thickness (h_2) being 5 μm and cell radius (r_c) being 12 μm [49]. The relationship between the calculated impedance of a single cell and r_c, h_2, membrane capacitance and cytoplasm resistivity (ρ_1) can be extracted from Eq. (12), as shown in Fig. S2. The model shows that cell morphology and electrical properties influence impedance. This model can provide a more quantitative relationship between the impedance and parameters related to the morphology and electrical properties of cells.

5. Conclusions

Sensor dimension influences the detection sensitivity of ECIS sensors. The experimental results reveal that smaller radius working electrodes generate more sensitive impedance responses to cell density change. Also, the smaller radius yields higher impedance values, which improves the signal-to-noise ratio. The counter electrodes need adequate sensing area to provide sufficient current paths for circuit connection. The distance between the edges of the sensing electrodes does not influence the measured impedance largely.

The proposed mathematical model was validated through experimental results and finite element analysis. This model can be used to calculate the distribution of electric potential and current over ECIS sensor electrodes. Also, it is able to provide a quantitative relationship between measured cell impedance and parameters

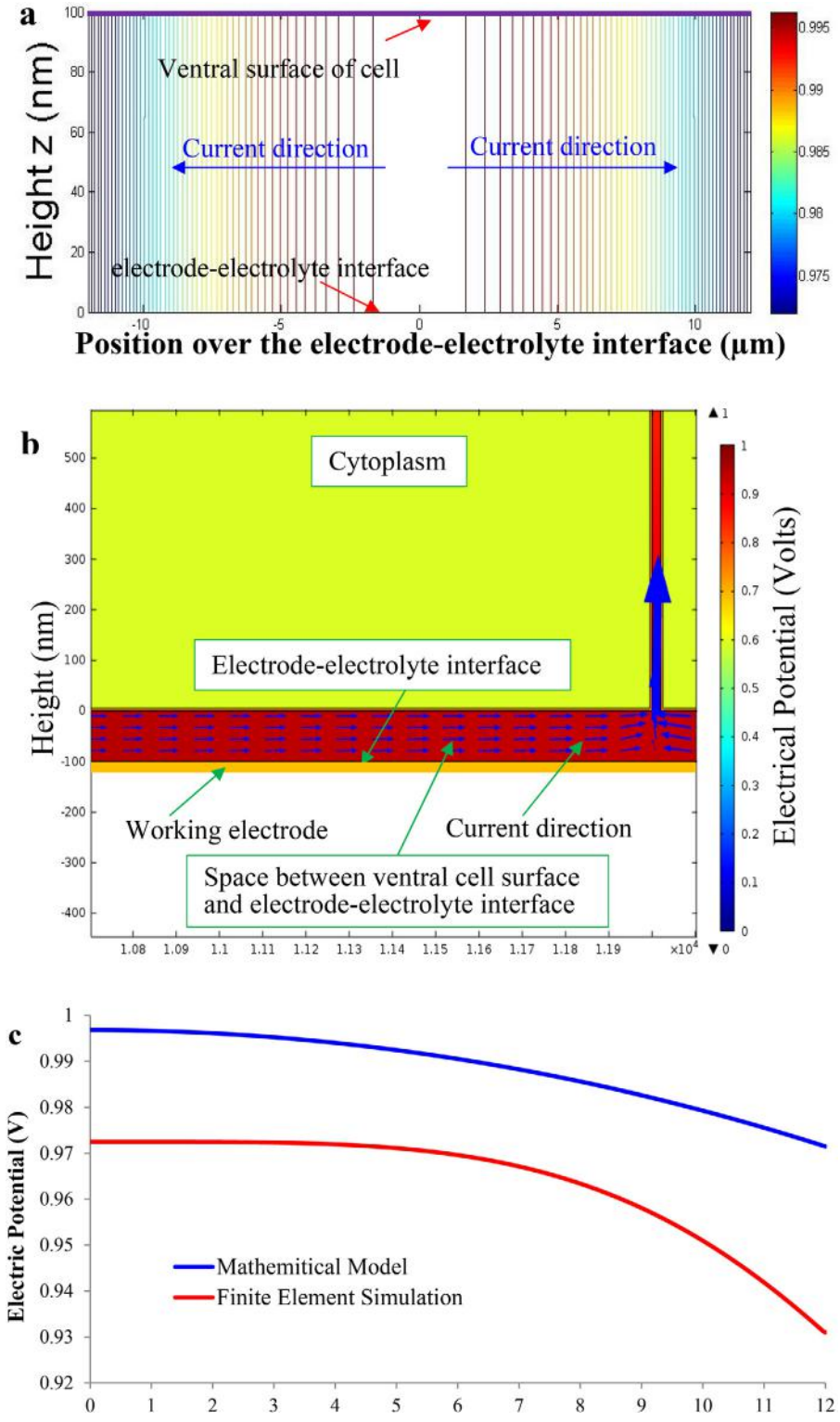

Fig. 8. (a) Distribution of equipotential lines in the space between the ventral cell surface and electrode–electrolyte interface layer. The axisymmetric axis of the cell locates at $x = 0$. (b) Current distribution between the ventral surface of cell and the electrode–electrolyte interface. The length and direction of blue arrows represent the current density and current direction. (c). Electric potential distributions between the ventral surface of the cell and the electrode–electrolyte interface calculated through the mathematical model and finite element simulation. (For interpretation of the references to color in this figure legend, the reader is referred to the web version of this article.)

including cell radius, thickness, membrane capacitance, and cytoplasm resistivity. This model can be used to optimize the design of ECIS sensors, such as the dimension of the working electrodes and the distance between the working electrode and counter electrode.

Acknowledgements

This work was supported by the US Army Research Office and Massachusetts Institute of Technology-Institute of Soldier

Nanotechnology (MIT-ISN) Historically Black Colleges Universities and Minority Institutions (HBCU-MI) program, award number: W911NF-13-D-0001, US Army Centre of Environmental Health Research (USACEHR), contract number: W81XWH-11-C-0026, and the Romanian Authority for Scientific Research through CNDI–UEFISCDI Grant PN-III-P2-2.1-PED-2016-1937. The content of the information does not necessarily reflect the position or the policy of the Government or MIT, and no official endorsement should be inferred. We also acknowledge the contributions from Andres Rivera, a undergraduate student at City College of New York, who helped us to design Figure 4.

Appendix A. Supplementary data

Supplementary material related to this article can be found, in the online version, at http://dx.doi.org/10.1016/j.snb.2017.03.047.

References

[1] I. Giaever, C. Keese, Monitoring fibroblast behavior in tissue culture with an applied electric field, Proc. Natl. Acad. Sci. U.S.A. 81 (1984) 3761–3764.
[2] I. Giaever, C.R. Keese, Use of electric fields to monitor the dynamical aspect of cell behavior in tissue culture, IEEE Trans. Biomed. Eng. (1986) 242–247.
[3] I. Giaever, C.R. Keese, Micromotion of mammalian cells measured electrically, Proc. Natl. Acad. Sci. U.S.A. 88 (1991) 7896–7900.
[4] C.R. Keese, K. Bhawe, J. Wegener, I. Giaever, Real-time impedance assay to follow the invasive activities of metastatic cells in culture, Biotechniques 33 (2002) 842–851.
[5] C.-M. Lo, C.R. Keese, I. Giaever, Cell–substrate contact: another factor may influence transepithelial electrical resistance of cell layers cultured on permeable filters, Exp. Cell Res. 250 (1999) 576–580.
[6] P. Mitra, C.R. Keese, I. Giaever, Electric measurements can be used to monitor the attachment and spreading of cells in tissue culture, Biotechniques 11 (1991) 504–510.
[7] C. Tiruppathi, A.B. Malik, P.J. Del Vecchio, C.R. Keese, I. Giaever, Electrical method for detection of endothelial cell shape change in real time: assessment of endothelial barrier function, Proc. Natl. Acad. Sci. U.S.A. 89 (1992) 7919–7923.
[8] C.-M. Lo, C.R. Keese, I. Giaever, Monitoring motion of confluent cells in tissue culture, Exp. Cell Res. 204 (1993) 102–109.
[9] Z. Pei, C.R. Keese, I. Giaever, H. Kurzawa, D.E. Wilson, Effect of the pSV2-neo plasmid on NIH 3T3 cell motion detected electrically, Exp. Cell Res. 212 (1994) 225–229.
[10] C.R. Keese, I. Giaever, A biosensor that monitors cell morphology with electrical fields, IEEE Eng. Med. Biol. Mag. 13 (1994) 402–408.
[11] H.E. Ayliffe, A.B. Frazier, R.D. Rabbitt, Electric impedance spectroscopy using microchannels with integrated metal electrodes, J. Microelectromech. Syst. 8 (1999) 50–57.
[12] A. Han, E. Moss, R.D. Rabbitt, K.L. Engisch, A.B. Frazier, A single cell multi-analysis system for electrophysiological studies, 12th International Conference on Solid-State Sensors, Actuators and Microsystems, TRANSDUCERS, IEEE2003 (2003) 674–677.
[13] A. Han, E. Moss, A.B. Frazier, Whole cell electrical impedance spectroscopy for studying ion channel activity, The 13th International Conference on Solid-State Sensors, Actuators and Microsystems, 2005 Digest of Technical Papers TRANSDUCERS'05, IEEE2005 (2005) 1704–1707.
[14] A. Han, L. Yang, A.B. Frazier, Quantification of the heterogeneity in breast cancer cell lines using whole-cell impedance spectroscopy, Clin. Cancer Res. 13 (2007) 139–143.
[15] K. Solly, X. Wang, X. Xu, B. Strulovici, W. Zheng, Application of real-time cell electronic sensing (RT-CES) technology to cell-based assays, Assay Drug Dev. Technol. 2 (2004) 363–372.
[16] Y. Qiu, R. Liao, X. Zhang, Real-time monitoring primary cardiomyocyte adhesion based on electrochemical impedance spectroscopy and electrical cell–substrate impedance sensing, Anal. Chem. 80 (2008) 990–996.
[17] K.S.-C. Ko, C.-M. Lo, J. Ferrier, P. Hannam, M. Tamura, B.C. McBride, et al., Cell–substrate impedance analysis of epithelial cell shape and micromotion upon challenge with bacterial proteins that perturb extracellular matrix and cytoskeleton, J. Microbiol. Methods 34 (1998) 125–132.
[18] J. Suehiro, R. Hamada, D. Noutomi, M. Shutou, M. Hara, Selective detection of viable bacteria using dielectrophoretic impedance measurement method, J. Electrostat. 57 (2003) 157–168.
[19] X. Zhang, F. Li, A.N. Nordin, J. Tarbell, I. Voiculescu, Toxicity studies using mammalian cells and impedance spectroscopy method, Sens. Biosens. Res. 3 (2015) 112–121.
[20] L. Wang, H. Wang, K. Mitchelson, Z. Yu, J. Cheng, Analysis of the sensitivity and frequency characteristics of coplanar electrical cell–substrate impedance sensors, Biosens. Bioelectron. 24 (2008) 14–21.
[21] L.J. Gentet, G.J. Stuart, J.D. Clements, Direct measurement of specific membrane capacitance in neurons, Biophys. J. 79 (2000) 314–320.
[22] S. Öz, C. Maercker, A. Breiling, Embryonic carcinoma cells show specific dielectric resistance profiles during induced differentiation, PLoS ONE 8 (2013) e59895.
[23] C.-M. Lo, C.R. Keese, I. Giaever, Impedance analysis of MDCK cells measured by electric cell–substrate impedance sensing, Biophys. J. 69 (1995) 2800.
[24] F. Asphahani, M. Zhang, Cellular impedance biosensors for drug screening and toxin detection, Analyst 132 (2007) 835–841.
[25] M.E. Spira, A. Hai, Multi-electrode array technologies for neuroscience and cardiology, Nat. Nanotechnol. 8 (2013) 83–94.
[26] H. Li, Q. Zou, L. Zou, Q. Wang, K. Su, N. Hu, et al., Detection of cardiovascular drugs and marine toxins using a multifunctional cell-based impedance biosensor system, Anal. Methods 7 (2015) 7715–7723.
[27] J. Wang, C. Wu, N. Hu, J. Zhou, L. Du, P. Wang, Microfabricated electrochemical cell-based biosensors for analysis of living cells in vitro, Biosensors 2 (2012) 127–170.
[28] S.E. Anderson, H.H. Bau, Electrical detection of cellular penetration during microinjection with carbon nanopipettes, Nanotechnology 25 (2014) 245102.
[29] P. Xue, J. Bao, Y.J. Chuah, N.V. Menon, Y. Zhang, Y. Kang, Protein covalently conjugated SU-8 surface for the enhancement of mesenchymal stem cell adhesion and proliferation, Langmuir 30 (2014) 3110–3117.
[30] J. Chen, Y. Zheng, Q. Tan, E. Shojaei-Baghini, Y.L. Zhang, J. Li, et al., Classification of cell types using a microfluidic device for mechanical and electrical measurement on single cells, Lab Chip 11 (2011) 3174–3181.
[31] J. Chen, Y. Zheng, Q. Tan, Y.L. Zhang, J. Li, W.R. Geddie, et al., A microfluidic device for simultaneous electrical and mechanical measurements on single cells, Biomicrofluidics 5 (2011) 014113.
[32] S. Park, Y. Zhang, T.-H. Wang, S. Yang, Continuous dielectrophoretic bacterial separation and concentration from physiological media of high conductivity, Lab Chip 11 (2011) 2893–2900.
[33] N.S. McNutt, R.S. Weinstein, The ultrastructure of the nexus A correlated thin-section and freeze-cleave study, J. Cell Biol. 47 (1970) 666–688.
[34] J. Bohnert, Effects of Time-varying Magnetic Fields in the Frequency Range 1 kHz to 100 kHz Upon the Human Body: Numerical Studies and Stimulation Experiment, KIT Scientific Publishing, 2014.
[35] Y. Iwanaga, Cell–Substrate Distance Measurement in Correlation With Distribution of Adhesion Molecules by Fluorescence Microscopy, Technische Universität München, 2000.
[36] Q. Lang, Y. Wu, Y. Ren, Y. Tao, L. Lei, H. Jiang, AC electrothermal circulatory pumping chip for cell culture, ACS Appl. Mater. Interfaces 7 (2015) 26792–26801.
[37] J.E.B. Randles, Kinetics of rapid electrode reactions, Discuss. Faraday Soc. 1 (1947) 11–19.
[38] H. Schwan, Electrode polarization impedance and measurements in biological materials, Ann. N.Y. Acad. Sci. 148 (1968) 191–209.
[39] E. Warburg, Ueber das Verhalten sogenannter unpolarisirbarer Elektroden gegen Wechselstrom, Annalen der Physik 303 (1899) 493–499.
[40] V.F. Lvovich, Impedance Spectroscopy: Applications to Electrochemical and Dielectric Phenomena, John Wiley & Sons, 2012.
[41] T.A. Nguyen, T.-I. Yin, D. Reyes, G.A. Urban, Microfluidic chip with integrated electrical cell-impedance sensing for monitoring single cancer cell migration in three-dimensional matrixes, Anal. Chem. 85 (2013) 11068–11076.
[42] W. Franks, I. Schenker, P. Schmutz, A. Hierlemann, Impedance characterization and modeling of electrodes for biomedical applications, IEEE Trans. Biomed. Eng. 52 (2005) 1295–1302.
[43] N. Joye, A. Schmid, Y. Leblebici, An electrical model of the cell–electrode interface for high-density microelectrode arrays, 2008 30th Annual International Conference of the IEEE Engineering in Medicine and Biology Society, IEEE2008 (2008) 559–562.
[44] Y.f. Alberto, O. Alberto, Cell Biometrics Based on Bio-Impedance Measurements, 2011.
[45] H.K. Henisch, Rectifying Semi-conductor Contacts, Clarendon Press, 1957.
[46] G.T. Kovacs, Introduction to the Theory, Design, and Modeling of Thin-film Microelectrodes for Neural Interfaces, Academic Press, San Diego, 1994, pp. 121–165.
[47] D.K. Schroder, Semiconductor Material and Device Characterization, John Wiley & Sons, 2006.
[48] A. Yúfera, A. Olmo, D. Cañete, P. Daza, Cell Biometrics Based on Bio-impedance Measurements, INTECH Open Access Publisher, 2011.
[49] W. Wang, Y. Sun, M. Zhang, R. Anderson, L. Langille, W. Chan, A system for high-speed microinjection of adherent cells, Rev. Sci. Instrum. 79 (2008) 104302.

Biographies

Xudong Zhang is a PhD candidate at the City University of New York. He received BS and MS degrees in Materials Science and Engineering from Jilin University, China, in 2006 and 2008 respectively. His research interests include electric cell–substrate impedance sensing (ECIS) technology, biosensor and microfluidic device design, fabrication, and application, mechatronic system design, and software development and programming.

William Wang has studied biology at Stanford University. He has researched at the Yale Medical School and City College of New York. His research focuses include biosensor, modeling and cancer cell signaling pathways.

Anis Nurashikin Nordin is an Associate Professor in International Islamic University Malaysia. She has a BS degree in Computer and Information Engineering from International Islamic University Malaysia in 1999. She obtained both MS and PhD degrees in Computer Engineering from the George Washington University, Washington, DC in 2002 and 2008 respectively. Her research area covers personalized healthcare devices, MEMS, BioMEMS, SAW devices, printed electronics, microfluidics.

Fang Li is an Assistant Professor of the Department of Mechanical Engineering at New York Institute of Technology. She received her BS and MS degrees in Precision Instruments from Tsinghua University, China, in 1999 and 2002 respectively, and her PhD degree in Mechanical Engineering from the University of Pittsburgh in 2008. After that, she developed an industrial career at Intelligent Automation, Inc. She joined the faculty at New York Institute of Technology since 2012. Prof. Li's research area covers biosensors, MEMS and NEMS, acoustic wave sensors, piezoelectric transducers, and non-destructive evaluations.

Sunghoon Jang is an Associate Professor and the chair of the CET Department at NY City College of Technology of CUNY. Dr. Jang received a master degree from New Jersey Institute of Technology (NJIT) in Electrical and Computer Engineering and a doctoral degree in Biomedical Engineering from University of Connecticut. His research areas of interest are in biomedical sensors & instrumentations, signal processing & control systems, and opto-electronics & laser optics. Professor Jang joined the ETET Department at City Tech in 2003 as an Assistant Professor, and became a faculty member of the CET Department in 2014. His current interests lie in non-invasive and minimally invasive optical and electro-chemical glucose sensors for diabetics and published numerous research papers and received research & academic grants within his areas of interest.

Ioana Voiculescu is an Associate Professor in the Mechanical Engineering Department, the City College of New York, New York. She received her PhD in Mechanical Engineering from the Technical University "Politehnica," Timisoara, Romania, and her ScD in Mechanical Engineering from the George Washington University, Washington, DC, in 2005. Since 2002, Dr. Voiculescu is a member of the ASME and IEEE. She published several journal papers in the area of microelectromechanical systems (MEMS) chemical and biological sensors. She also has two patents in her name.